

Dynamical Nuclear Polarization by Electrical Spin Injection in Ferromagnet-Semiconductor Heterostructures

J. Strand,¹ B. D. Schultz,² A. F. Isakovic,¹ C. J. Palmström,² and P. A. Crowell^{1,*}

¹*School of Physics and Astronomy*

²*Department of Chemical Engineering and Materials Science,
University of Minnesota, Minneapolis, MN 55455*

Electrical spin injection from Fe into $\text{Al}_x\text{Ga}_{1-x}\text{As}$ quantum well heterostructures is demonstrated in small (< 500 Oe) in-plane magnetic fields. The measurement is sensitive only to the component of the spin that precesses about the internal magnetic field in the semiconductor. This field is much larger than the applied field and depends strongly on the injection current density. Details of the observed hysteresis in the spin injection signal are reproduced in a model that incorporates the magnetocrystalline anisotropy of the epitaxial Fe film, spin relaxation in the semiconductor, and the dynamical polarization of nuclei by the injected spins.

PACS numbers: 72.25.Hg, 72.25.Rb, 76.60.Jx

The injection of spin from a conventional ferromagnetic metal into a semiconductor is a prerequisite for several proposed magneto-electronic devices [1]. Although spin transport across the ferromagnet-semiconductor (FM-S) interface has recently been demonstrated [2, 3, 4, 5], most injection experiments on metallic FM-S systems have required relatively large magnetic fields, in excess of several kilogauss, to produce a spin component *perpendicular* to the FM-S interface. The most useful properties of typical ferromagnetic thin films, however, such as low-field switching and hysteresis, can be exploited only by coupling to the *in-plane* component of the magnetization [6]. In the case of metallic FM-S structures, in-plane coupling has been observed only as a small change in transport properties [2] or using optically pumped carriers [7, 8].

In this Letter we report a demonstration of electrical spin injection in FM-S heterostructures using small (< 500 Oe) in-plane magnetic fields. We measure only the component of the spin that precesses after injection into the semiconductor using electroluminescence polarization (ELP) as a detection technique [6, 9]. The effective magnetic field inducing the precession depends strongly on the electrical bias conditions and is dramatically enhanced at the highest injection current densities. The origin of the hysteresis in the spin polarization signal is magnetization reversal in the ferromagnet, but the magnitude and shape of the observed loops depend on the effective field in the semiconductor. Modeling based on the results of optical pumping experiments demonstrates that the origin of the large effective field is dynamical nuclear polarization due to the spin-polarized current injected from the ferromagnet [10]. This approach to dynamical nuclear polarization in semiconductors is a simple alternative to the use of optical pumping or high magnetic fields as sources of spin-polarized electrons [11, 12].

We report results from two heterostructures with different quantum well (QW) spin detectors. The samples are grown by molecular beam epitaxy on p^+ GaAs (100) substrates and consist of $\text{p-Al}_x\text{Ga}_{1-x}\text{As}/\text{QW}/\text{n-}$

$\text{Al}_x\text{Ga}_{1-x}\text{As}/\text{Fe}/\text{Al}$ [13]. Intrinsic setback layers are placed on both sides of the QW, and the resulting p-i-n structure forms a light-emitting diode (LED). The 50 Å thick iron and the 25 Å Al layers are grown *in situ* at $\approx 0^\circ$ C. A Si δ -doped layer ($\delta = 2 \times 10^{13}$ atoms/cm² for sample A and 3×10^{13} atoms/cm² for sample B) is grown 25 Å below the Fe-semiconductor interface in order to form a tunneling contact. For sample A, $x = 0.2$ and the QW is 100 Å $\text{Al}_{0.1}\text{Ga}_{0.9}\text{As}$ with p-doped barriers. For sample B, $x = 0.1$ and the QW is 100 Å GaAs with intrinsic barriers. The important difference between the samples is the effective g -factor g^* for electrons in the QW. For sample B, $g^* \approx -0.4$, while sample A was designed to have an electron g -factor close to zero [14]. The magnetocrystalline anisotropy of the epitaxial Fe film results in easy and hard axes along $[011]$ and $[01\bar{1}]$, as shown in Fig. 1.

The samples are processed into 200 μm wide mesas. The ferromagnetic contact is 80 μm wide, and a 40 μm wide gold contact is evaporated over the center of the bar, which is cleaved into pieces 1–1.5 mm long. The devices are operated with the Schottky contact under reverse bias and the p-i-n LED under forward bias. Electrons tunnel from the Fe into the n-layer and recombine in the QW with holes supplied by the substrate. Electroluminescence (EL) is collected along the sample normal $\hat{\mathbf{z}}$, and is dominated by heavy-hole recombination. Under these conditions the circular polarization of the EL, which we will refer to as the ELP signal, is equal to the electron spin polarization along $\hat{\mathbf{z}}$ at the time of recombination [15].

In a typical ELP measurement in the Faraday geometry, $\hat{\mathbf{k}} \parallel \hat{\mathbf{z}} \parallel \mathbf{B}_a$, where $\hat{\mathbf{k}}$ is the direction of light propagation, and \mathbf{B}_a is the applied magnetic field [3, 4]. The inset of Fig. 1 shows the ELP signal measured in the Faraday geometry for sample A. The observed signal is proportional to the magnetization of the Fe film and is significantly larger than the background determined by either the photoluminescence (PL) polarization measured

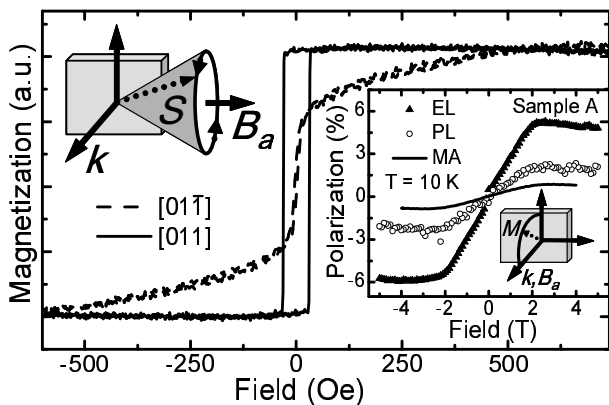


FIG. 1: In-plane magnetization of the epitaxial Fe film (sample A) parallel to fields applied along $[011]$ and $[01\bar{1}]$. Left inset: schematic of Voigt geometry experimental setup. The direction of light propagation \hat{k} is along the sample normal, \mathbf{B}_a is the applied field, and \mathbf{S} is the precessing spin in the semiconductor. Right inset: Faraday geometry data and experimental setup. \mathbf{M} is the magnetization of the Fe film. The three curves show electroluminescence (EL), photoluminescence (PL), and magnetoabsorption (MA) polarization as a function of the magnetic field \mathbf{B}_a applied along \hat{z} .

at a bias just below the EL threshold or the magnetoabsorption (MA) of the Fe film. This result indicates a steady-state spin polarization in the QW of at least 4% for applied fields above 2.1 T, the saturation field for Fe.

In the transverse field configuration ($\hat{k} \parallel \hat{z} \perp \mathbf{B}_a$) shown in the left inset of Fig. 1, the magnetocrystalline anisotropy of the Fe film allows for a significant angle between the electron spin \mathbf{S} and \mathbf{B}_a . The magnetization remains in the sample plane and \mathbf{S} precesses out of the plane after injection into the semiconductor. This approach is related philosophically to the oblique Hanle effect [15], in which optically pumped spins are created at an angle $0 < \theta < \pi/2$ with respect to the applied field, an approach followed in the recent electrical spin injection experiment of Motsnyi *et al.* [5]. An important advantage of our approach is that we detect only the precessing component of the spin, making the measurement essentially immune to background effects.

Figures 2(a) and (b) show the ELP signal as a function of the transverse magnetic field, which is applied in the sample plane at a small angle ($4^\circ \pm 2^\circ$) from the $[01\bar{1}]$ axis. Data are shown at several different current densities for samples A and B. At the lowest current densities, just above the threshold for light emission, the ELP signal is nearly independent of the applied magnetic field and shows no hysteresis, although there is a polarization offset of 0 - 2.5%. As the current density is increased, a double loop structure develops. In the case of sample A [Fig. 2(a)], the magnitude of the polarization signal increases with increasing bias, reaching a maximum value of approximately 4%, determined from the peak-to-peak

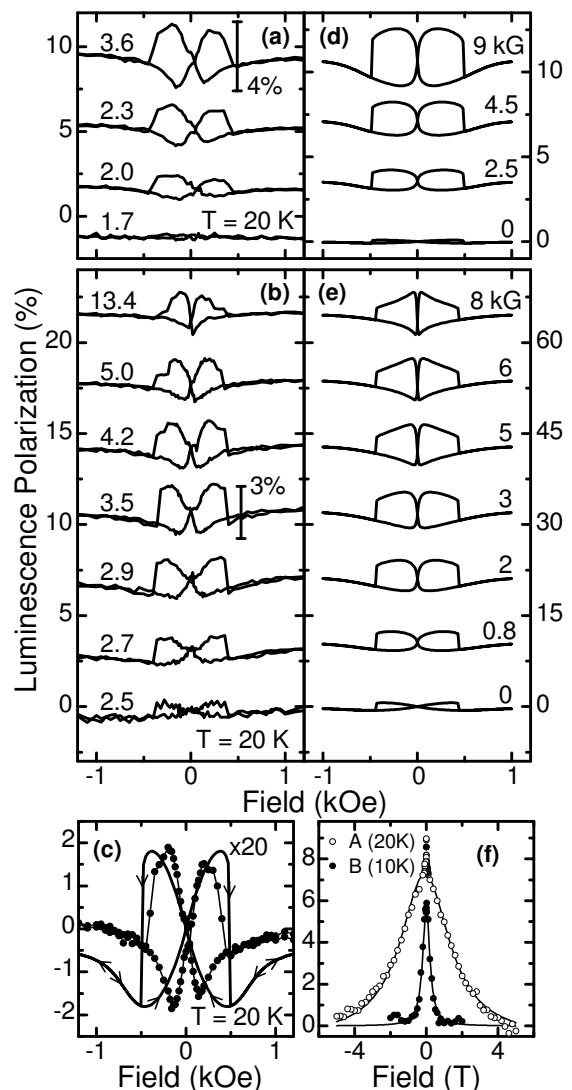


FIG. 2: (a), (b) Electroluminescence polarization (ELP) as a function of field applied at $4^\circ \pm 2^\circ$ to $[01\bar{1}]$ for samples A and B, respectively, at several current densities. Each curve is labeled by the current density in units of A/cm^2 . (c) Sample A ELP (points) as a function of field, with a -2.15% offset removed, and model ELP signal (solid curve) scaled by a factor of 20. (d), (e) Model ELP signal, including the effective nuclear field, as a function of applied field for samples A and B, respectively. The curves are labeled by the effective field b_N in kG (see Eq. 2). (f) Hanle curves measured for samples A and B. Curves in (a), (b), (d) and (e) are offset for clarity.

height of the loop. In the case of sample B [Fig. 2(b)], both the magnitude *and the shape* of the observed loops depend on the current density. A maximum in the signal is observed at a current density of approximately $3.5 \text{ A}/\text{cm}^2$, above which the signal decreases and the central dip in the loop becomes much narrower. Photoluminescence measurements on the same structures show no polarization signal in a transverse magnetic field.

The origin of the ELP signal observed in Fig. 2 is pre-

cession of the spin injected from the ferromagnet. The observed polarization depends on the angle between \mathbf{B}_a and the magnetization \mathbf{M} of the Fe film as well as the precession frequency and spin relaxation time in the QW. Under the assumption that the magnetization reversal in the Fe film occurs by coherent rotation [16], the angle between \mathbf{M} and \mathbf{B}_a , and hence the orientation of the injected spin \mathbf{S}_0 can be determined from the magnetization data. The spin dynamics in the semiconductor are modeled using the formalism developed for the optical Hanle effect [15]:

$$\frac{d\mathbf{S}}{dt} = \frac{\mathbf{S}_0}{\tau} - \frac{\mathbf{S}}{\tau_s} - \frac{\mathbf{S}}{\tau} + \boldsymbol{\Omega} \times \mathbf{S}, \quad (1)$$

where τ_s^{-1} is the spin relaxation rate, τ^{-1} is the recombination rate, and $\boldsymbol{\Omega} = g^* \mu_B \mathbf{B} / \hbar$, where μ_B is the Bohr magneton.

The steady-state spin \mathbf{S} that is measured by ELP can be found from Eq. 1 by setting $d\mathbf{S}/dt = 0$. We will be interested in an upper bound for \mathbf{S} and will hence assume that $\mathbf{S}_0 = \epsilon \hat{\mathbf{m}}$, where $\epsilon = 0.42$ is the spin polarization of Fe [17] and $\hat{\mathbf{m}}$ is a unit vector parallel to \mathbf{M} . The parameters in Eq. 1 are thus reduced to two: the ratio $\alpha = \tau_s / \tau$, and a characteristic field scale $B_{1/2} = \hbar / (\mu_B g^* T_s)$, where $T_s^{-1} = \tau_s^{-1} + \tau^{-1}$. We determine α and $B_{1/2}$ by fitting the results of Hanle effect measurements, in which electron spins are optically injected along $\hat{\mathbf{z}}$ using circularly polarized light tuned near the band-edge of the QW barriers. The circular polarization of the PL as a function of the transverse magnetic field is shown for both samples in Fig. 2(f). Fits to the expected Lorentzian shape [15] are shown as the solid curves. The dramatic difference in the widths of the two Hanle curves is due primarily to the different electron g -factors in the two quantum wells.

Once the magnetization of the ferromagnet and the Hanle curve are known for each sample, it is then possible to model the ELP signal without any free parameters. The result for sample A is shown as the solid curve in Fig. 2(c) along with data obtained at a current density of 3.6 A/cm². (A field-independent offset has been removed from the experimental data.) The ELP signal vanishes at large applied fields because the injected spin is parallel to the field, and the signal vanishes at zero field because there is no precession. At intermediate fields, the magnetization is between the easy and hard axes, and the non-zero angle between \mathbf{S}_0 and \mathbf{B}_a results in an ELP signal.

In spite of the general qualitative agreement in Fig. 2(c), the magnitude of the signal determined from our model is *smaller* than the experimental result by a factor of ≈ 20 , even though we have already assumed a spin injection efficiency of unity. More significantly, the model of Eq. 1 cannot replicate the current-driven change in the shape of the ELP loops observed for sample B without requiring either the spin lifetimes or g^* to

increase by over an order of magnitude with increasing bias.

The most probable explanation for the discrepancy between the simple dynamical model and the experiment is that the effective magnetic field in the semiconductor is larger than the applied field and depends on the current density. This hypothesis is motivated by the observation of large internal magnetic fields in optical pumping experiments due to dynamical nuclear polarization (DNP) by electron spins [18, 19]. In our experiment, the spins are injected electrically, and the magnitude of the nuclear polarization is determined by the current density [10]. The total magnetic field for electron spins is then the sum of the applied field \mathbf{B}_a and a nuclear field [18]

$$\mathbf{B}_N = b_N \frac{(\hat{\mathbf{s}} \cdot \mathbf{B}_a) \mathbf{B}_a}{B_a^2 + B_0^2}, \quad (2)$$

where $\hat{\mathbf{s}}$ is a unit vector parallel to the injected spin, B_0 is the nuclear dipolar field and b_N is the maximum nuclear field. We set B_0 to 2 G, a typical value for GaAs [18], and allow b_N to vary with current density. The total field $\mathbf{B} = \mathbf{B}_a + \mathbf{B}_N$ is then used in Eq. 1 to determine \mathbf{S} and the expected ELP signal. The results of modeling with a nuclear field, adjusting b_N as the only free parameter, are shown in Figs. 2(d) and (e). Agreement with the magnitude of the experimental results is obtained using values of b_N between 0 and 9 kG, which are indicated next to each curve. These are comparable to the internal fields obtained in optical pumping experiments and are well below the maximum possible internal field of 5.3 T [18, 20].

Including the effects of DNP also accounts for the major differences between the ELP curves observed for samples A and B. Although the shape of the ELP loops is nearly independent of current density for sample A, the position of the maximum signal observed for sample B shifts toward zero field as the current density increases, and the jump observed at larger applied fields disappears. The same trend is observed in the theoretical curves. The difference in behavior reflects the fact that the magnetization reversal in the two samples is essentially the same, while the widths of the Hanle curves differ by a factor of six. In the case of sample A, the total internal field is less than the half-width of the Hanle curve. In this case, the average spin precesses only a fraction of a cycle before recombination, and the shape of the ELP loop is determined only by the rotation of the magnetization in the ferromagnet. In contrast, the maximum nuclear field in sample B exceeds the half-width of the Hanle curve, and hence spin precession in the semiconductor changes the shape of the ELP signal as well as determining its magnitude.

Given that only one parameter was varied to obtain the theoretical curves shown in Fig. 2, the overall agreement with the experiment provides strong support for DNP

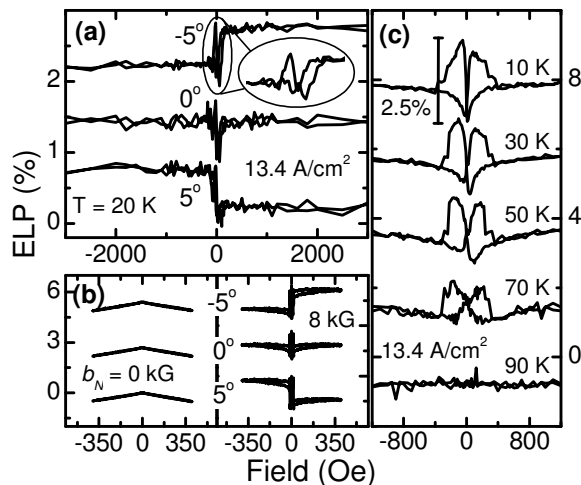


FIG. 3: (a) Sample B electroluminescence polarization (ELP) data as a function of magnetic field for directions close to the [011] axis. The field is applied in the (100) plane (middle), and $\pm 5^\circ$ out of the (100) plane (top and bottom curves). There is an in-plane rotation of 5° in all three cases. The inset shows an expansion of the region near zero field. (b) Modeling of results for this geometry without (left) and with (right) the nuclear field. (c) ELP signal for sample B as a function of magnetic field applied along $[01\bar{1}]$ at several different temperatures. All curves are offset for clarity.

by electrical spin injection. The most important discrepancy between the data and the model occurs near zero field, where the suppression of the experimental signal occurs over a much wider field range than in the model. The narrow region observed in the model is based on the nuclear dipole field of 2 G for bulk GaAs. However, the suppression of DNP over a much wider field range has been observed in optical pumping studies of ferromagnet-semiconductor interfaces [7] and quantum dots [21]. Furthermore, the behavior near zero field is very sensitive to the details of the magnetic reversal process which may not be described completely by the simple coherent rotation model.

Additional evidence for the existence of a nuclear field comes from data obtained for fields applied near the [011] axis. As can be seen from the square hysteresis loop shown in Fig. 1, the magnetization along this direction is essentially parallel to \mathbf{B}_a for any field, and in this case the torque term in Eq. 1 is zero. As a result, no precession is expected. This is consistent with the behavior observed in the middle curve of Fig. 3(a), which was obtained for a magnetic field applied in the (100) plane at an angle of 5° with respect to [011]. The top and bottom curves in Fig. 3(a) were obtained for rotations of the field axis $\pm 5^\circ$ out of the (100) plane. The curves in Fig. 3(b) are the results of the model of Eq. 1 using only the applied field (left) and including the nuclear field from Eq. 2 (right). The effective field b_N of 8 kG is the same as that used to fit the hard axis data at the same current density, and

the raw magnetization data were used to determine the direction of \mathbf{S}_0 . As can be seen in Figs. 3(a) and (b), there is good agreement with the experiment *only* if the nuclear field is included. The extreme sensitivity of the modeling results to the presence of the nuclear field in the easy axis case follows from the dot product $\hat{\mathbf{s}} \cdot \mathbf{B}_a$ in Eq. 2. This compensates for the fact that the torque term in Eq. 1 nearly vanishes for small angles between \mathbf{S} and \mathbf{B}_a . The dip in the signal at zero field shown in the inset of Fig. 3(a) is due to dipolar relaxation.

The efficiency of the DNP process should decrease with increasing temperature [22]. A strong suppression of the ELP signal with increasing temperature is seen in both samples and is shown for sample B in Fig. 3(c). The change in the shape of the ELP hysteresis loop with temperature also mirrors the dependence on current density seen in Fig. 2.

The approach to spin injection outlined in this Letter realizes the possibility of using conventional ferromagnets, small magnetic fields, and DC electrical currents to create and manipulate spin polarized carriers in a semiconductor device. There remain several open questions, including a microscopic description of the DNP mechanism and its relation to the injection process. This will require a more detailed study of the transport properties of these systems, with the goal of achieving a purely electronic means of spin detection.

We acknowledge L. J. Sham and C. Ciuti for helpful discussions. This work was supported by ONR, the DARPA/ONR SPINS program, the University of Minnesota MRSEC (NSF DMR-0212032), and the Institute for Rock Magnetism. A.F.I. and B.D.S thank 3M for fellowship support.

* Electronic address: crowell@physics.umn.edu

- [1] S. Datta and B. Das, *Appl. Phys. Lett.* **56**, 665 (1990).
- [2] P. R. Hammar, B. R. Bennett, M. J. Yang, and M. Johnson, *Phys. Rev. Lett.* **83**, 203 (1999).
- [3] H. J. Zhu *et al.*, *Phys. Rev. Lett.* **87**, 016601 (2001).
- [4] A. T. Hanbicki *et al.*, *Appl. Phys. Lett.* **80**, 1240 (2002).
- [5] V. F. Motsnyi *et al.*, *Appl. Phys. Lett.* **81**, 265 (2002).
- [6] Y. Ohno *et al.*, *Nature* **402**, 790 (1999).
- [7] R. K. Kawakami *et al.*, *Science* **294**, 131 (2001).
- [8] R. J. Epstein *et al.*, *Phys. Rev. B* **65**, 121202 (2002); R. J. Epstein *et al.*, unpublished.
- [9] R. Fiederling *et al.*, *Nature* **402**, 787 (1999).
- [10] M. Johnson, *Appl. Phys. Lett.* **77**, 1680 (2000).
- [11] J. H. Smet *et al.*, *Nature* **415**, 281 (2002).
- [12] S. E. Barrett, R. Tycko, L. N. Pfeiffer, and K. W. West, *Phys. Rev. Lett.* **72**, 1368 (1994).
- [13] A. F. Isakovic *et al.*, unpublished.
- [14] D. J. Chadi, A. H. Clark, and R. D. Burnham, *Phys. Rev. B* **13**, 4466 (1976).
- [15] M. I. Dyakonov and V. I. Perel, in *Optical Orientation*, edited by F. Meier and B. P. Zakharchenya (North-Holland Physics Publishers, New York, 1984).

- [16] E. C. Stoner and E. P. Wohlfarth, *Philos. Trans. R. Soc. A* **240**, 599 (1948).
- [17] R. Meservey and P. M. Tedrow, *Phys. Rep.* **238**, 173 (1994).
- [18] D. Paget, G. Lampel, B. Sapoval, and V. I. Safarov, *Phys. Rev. B* **15**, 5780 (1977).
- [19] G. P. Flinn *et al.*, *Semicond. Sci. Technol.* **5**, 533 (1990).
- [20] G. Salis, D. D. Awschalom, Y. Ohno, and H. Ohno, *Phys. Rev. B* **64**, 195304 (2001).
- [21] D. Gammon *et al.*, *Phys. Rev. Lett.* **86**, 5176 (2001).
- [22] A. Abragam, *Principles of Nuclear Magnetism* (Oxford Univ. Press, Oxford, 1961).